

The impact of environment on the dynamical structure of satellite systems

A. Faltenbacher^{1,2,3} *

¹*Physics Department, University of the Western Cape, Cape Town 7535, South Africa*

²*Max-Planck-Institute for Astrophysics, Karl-Schwarzschild-Str. 1, D-85741 Garching, Germany*

³*MPA/SHAO Joint Center for Astrophysical Cosmology at Shanghai Astronomical Observatory, Nandan Road 80, Shanghai 200030, China*

7 February 2020

ABSTRACT

We examine the impact of environment on the dynamical structure of satellite systems based on the Millennium–II Simulation. Satellite halos are defined as sub–halos within the virial radius of a host halo. The satellite sample is restricted to those sub–halos which showed a maximum circular velocity above 30 km s^{-1} at the time of accretion. Host halo masses range from 10^{10} to $10^{14} h^{-1} M_{\odot}$. We compute the satellites’ average accretion redshift, z_{acc} , velocity dispersion, σ , and velocity anisotropy parameter, β , utilising stacked satellite samples of equal mass hosts at similar background densities. The main results are: (1) On average satellites within hosts in high density environments are accreted earlier ($\Delta z \approx 0.1$) compared to their counterparts at low densities. For host masses above $5 \times 10^{13} h^{-1} M_{\odot}$ this trend weakens and may reverse for higher host masses; (2) The velocity dispersion of satellites in low density environments follows that of the host, i.e. no velocity bias is observed for host halos at low densities independent of host mass. However, for low mass hosts in high density environments the velocity dispersion of the satellites can be a few times larger than that of the host halo, i.e. the satellites are dynamically hotter than their host halos. (3) The anisotropy parameter depends on host mass and environment. Satellites of massive hosts show more radially biased velocity distributions. Moreover in low density environments satellites have more radially biased velocities ($\Delta\beta \gtrsim 0.1$) compared to their counterparts in high density environments. We believe that our approach allows one to predict a similar behaviour for observed satellite galaxy systems.

Key words: methods: N-body simulations — methods: numerical — dark matter — galaxies: haloes — galaxies: clusters: general

1 INTRODUCTION

The dependence of halo statistics on a second parameter in addition to mass is now generally referred to as assembly bias. Simple extensions to the Press–Schechter and excursion set models (Press & Schechter 1974; Kaiser 1984; Bond et al. 1991; Cole & Kaiser 1989; Lacey & Cole 1993; Mo & White 1996) predict the clustering of halos to depend on their mass alone. However, Gao et al. (2005) and various subsequent studies showed that clustering also depends on other halo properties, for example, formation time, concentration, substructure content, spin and shape (Harker et al. 2006; Wechsler et al. 2006; Bett et al. 2007; Gao & White 2007; Jing et al. 2007; Macciò et al. 2007; Wetzel et al. 2007; Angulo et al. 2008). Using a mass filter in configuration space rather than in k-space Zentner

(2007) demonstrated that excursion set models predict that halos in denser environments do form later, independent of halo mass. At the high mass end this agrees with findings from N-body simulations (e.g., Wechsler et al. 2002; Jing et al. 2007), but is opposite to the behaviour observed at the low mass end. Based on statistics of the peaks within Gaussian random fluctuations, Dalal et al. (2008) argued that the behaviour for low mass halos can be understood if cessation of mass accretion is taken into account.

Several other studies have investigated the dependence of halo formation times or, similarly, merger rates on environment (e.g., Gottlöber et al. 2001, 2002; Sheth & Tormen 2004; Fakhouri & Ma 2009a,b; Hahn et al. 2007). Although slightly different density estimators are employed, such as over density in a sphere or mark correlation functions, it is generally agreed upon that halos less massive than $\sim 10^{13} h^{-1} M_{\odot}$, which reside in high density regions, form

* E-mail:afaltenbacher@uwc.ac.za

earlier compared to those with equal mass but located in less dense regions.

In a preceding study we discussed the dependence of the dynamical structure of dark matter halos on environment (Faltenbacher & White 2009). We have found that the velocity dispersion of dark matter halos residing in less dense environments shows a more radially biased velocity structure compared to halos of the same mass in denser environments. We now extend this study to the dynamics of satellites within host halos. Satellites are selected on the basis that our findings can be applied to observed satellite galaxy systems. The effects of environment on the dynamical structure of satellites may have important implications for the accretion processes of the host galaxies.

The outline of the paper is as follows. In § 2 we introduce the simulation and the halo finding procedure. We then explain how the environment of host halos is determined and describe the stacking procedure to compute average properties of satellite populations. § 3 presents the results: host halo properties as a function of environment are shown in § 3.1; main results are portrayed in § 3.2 where we discuss the accretion history and dynamical structure of satellite systems. In § 3.3 we investigate resolution effects. A conclusion is given in § 4.

2 METHODOLOGY

In this section we describe the tools for our analysis. A short account on the Millennium-II Simulation is followed by the discussion of the halo finding procedure. We also explain the determination of the background density and the stacking procedure used to derive averaged properties of satellite systems in different environments.

2.1 Simulation

The Millennium-II Simulation (Boylan-Kolchin et al. 2009; Springel 2005) adopted concordance values for the parameters of a flat Λ cold dark matter (Λ CDM) cosmological model, $\Omega_{\text{dm}} = 0.205$ and $\Omega_{\text{b}} = 0.045$ for the current densities in CDM and baryons, $h = 0.73$ for the present dimensionless value of the Hubble constant, $\sigma_8 = 0.9$ for the rms linear mass fluctuation in a sphere of radius $8 h^{-1} \text{Mpc}$ extrapolated to $z = 0$, and $n = 1$ for the slope of the primordial fluctuation spectrum. The simulation followed 2160^3 dark matter particles from $z = 127$ to the present day within a cubic region $100 h^{-1} \text{Mpc}$ on a side resulting in individual particle masses of $6.9 \times 10^6 h^{-1} M_{\odot}$. The gravitational force had a Plummer-equivalent comoving softening of $1 h^{-1} \text{kpc}$. We refer readers to Boylan-Kolchin et al. (2009) for more detailed description of the simulation.

2.2 Halo sample and accretion times

The halos are found by a two-step procedure. In the first step all collapsed halos with at least 20 particles are identified using a friends-of-friends (fof) group-finder with linking parameter $b = 0.2$. These objects will be referred to as fof-halos. Then post-processing with the substructure

algorithm SUBFIND (Springel et al. 2001) subdivides each fof-halo into a set of self-bound sub-halos. Sub-halos with less than 20 particles are discarded. Here we consider the most prominent sub-halo within each fof-halo as host halo. To characterise a host halo we use: the maximal circular velocity, V_{max} , which peaks at a radius, R_{max} ; the concentration, $c_{\text{max}} = R_{\text{vir}}/R_{\text{max}}$, where R_{vir} denotes the virial radius which comprises a mean density of 94 times the critical value. If one assumes a Navarro-Frenk-White like density profile (Navarro et al. 1997), R_{max} is a factor of ~ 2.1 larger than the scale radius R_{s} , which has conventionally been used to compute the concentration; and the three dimensional velocity dispersion, σ_{3D} , which we scale for each halo individually by the virial velocity, $V_{\text{vir}} = (GM_{\text{vir}}/R_{\text{vir}})^{\frac{1}{2}}$, where M_{vir} is the virial mass and G is the gravitational constant.

Besides the *host halo*, all other sub-halos within the virial radius are referred to as *satellite halos*. The accretion redshift of a satellite halo onto the host halo is determined as the redshift at which it discontinues to be the most prominent sub-halo in its own fof-halo. We define the redshift of the snapshot just prior to accretion as *accretion redshift*. This typically corresponds to the time when the halo acquires the maximum mass during the course of its evolution (cf., Guo et al. 2009). With $V_{\text{max,acc}}$ we denote the maximum circular velocity of the halo at that time. Following Kravtsov et al. (2004) we include only those satellite halos in our analysis with $V_{\text{max,acc}} \geq 30 \text{ km s}^{-1}$. Halos with lower masses presumably contain only negligible amounts of stars. We suspend this requirement only for a resolution study in § 3.3.

2.3 The background density field

The background density field is computed based on all sub-halos with maximum circular velocities, V_{max} , between 200 km s^{-1} and 300 km s^{-1} . As Figure 1 illustrates, this velocity range corresponds to halo masses close to $M_* = 6.15 \times 10^{12} h^{-1} M_{\odot}$ which is the typical collapse mass at $z = 0$ for the given cosmology. Halos in this mass range provide a relatively unbiased sampling of the overall density field. We denote these halos as V_* -halos. To facilitate the comparison with density estimates based on observed galaxies we include all sub-halos within the given velocity range irrespective of whether they are host or satellite halos. In total there are 2013 V_* halos resulting in a sampling of the density field based on a point set with a mean distance of slightly less than $8 h^{-1} \text{Mpc}$.

The background density for any given halo is determined by the seven nearest V_* halos, each of them smoothed with a smoothing kernel of the form (Monaghan & Lattanzio 1985)

$$W(r; h) = \frac{8}{\pi h^3} \begin{cases} 1 - 6 \left(\frac{r}{h}\right)^2 + 6 \left(\frac{r}{h}\right)^3, & 0 \leq \frac{r}{h} \leq \frac{1}{2}, \\ 2 \left(1 - \frac{r}{h}\right)^3, & \frac{1}{2} < \frac{r}{h} \leq 1, \\ 0, & \frac{r}{h} > 1. \end{cases} \quad (1)$$

As in Springel et al. (2001) we define the smoothing kernel on the interval $[0, h]$ and not on $[0, 2h]$ as frequently done in the literature. The background density at a given halo

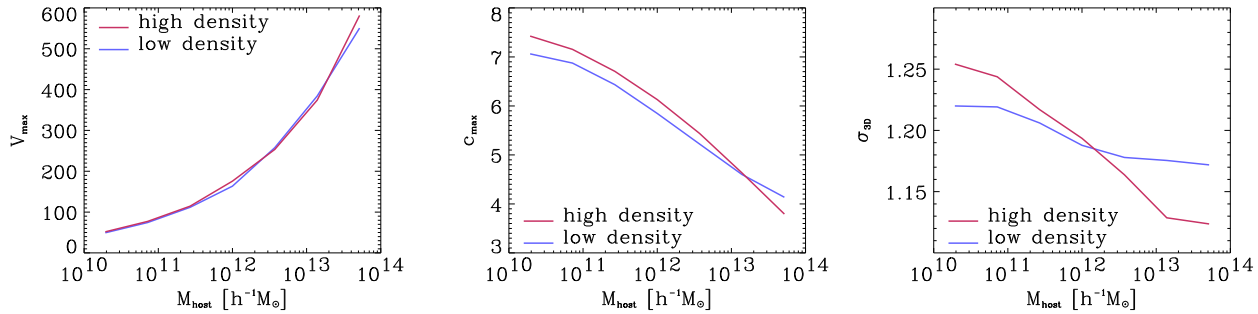


Figure 1. Average host halo properties, maximum circular velocity (V_{max}), concentration (c_{max}) and 3D velocity dispersion (σ_{3D}), as a function of halo mass. Red and blue lines display results based on halos in the upper and lower 33% tails of their background density distributions. Halo concentrations, c_{max} , are defined as the ratio of the virial mass to the radius of the maximum circular velocity. Before averaging the velocity dispersion of each individual halo is scaled by its virial velocity, $V_{\text{vir}} = (GM_{\text{vir}}/R_{\text{vir}})^{1/2}$.

location is the sum of the contributions of the seven nearest neighbours. Using this recipe, a *background density* is assigned to each host halo which we also address as *environment* of the host. In the subsequent analysis the host halos are ordered according to their background density and average properties of the upper and lower 33% tails are determined separately. We also investigated the outcome based on the upper and lower 20% tails and found very similar results. To improve statistics we choose the larger background density intervals.

2.4 The stacking procedure

Besides deriving the average accretion redshift, z_{acc} , of the satellite populations as a function of host mass and environment, we aim to study differences in their average dynamical properties. To achieve reasonable statistical significance individual host halos with similar masses and background densities are stacked. Since the mass bins have a certain width the host masses in a given mass bin vary. In order to increase accuracy we scale the satellite velocities before stacking. In particular we employ the virial velocity, V_{vir} , to scale the satellites' velocities.

The scaled velocities of satellites belonging to host halos of a given mass at a given background density are used to compute the mean radial velocity, v_{rad} , the three dimensional velocity dispersion, σ_{3D} , its radial and tangential components, σ_{rad} and σ_{tan} , and based on these quantities the velocity anisotropy parameter, $\beta = 1 - 0.5(\sigma_{\text{tan}}^2/\sigma_{\text{rad}}^2)$. In addition we compute the average number of satellites, N_{sat} , as a function of host mass and environment as well as the average ratio between the actual maximal circular velocity and that one at the time of the satellites' accretion, $V_{\text{max}}/V_{\text{max,acc}}$.

3 RESULTS

Before we discuss the environment dependence of accretion times and dynamical structure of satellite systems we review the impact of environment on the host halo properties themselves. Resolution effects are discussed in the final paragraph.

3.1 Host halo properties as a function of environment

The left panel of Figure 1 shows the average maximum circular velocity, V_{max} , of host halos as a function of mass. Red and blue lines, as with all the remaining figures, show the result for the halos within the upper and lower 33% tails of the background density distributions. Subsequently, we will address the two samples as *high* and *low* density samples. The figure indicates that the average values of V_{max} are independent of environment.

The middle panel of Figure 1 displays the concentration, c_{max} , as a function of host mass and environment. In agreement with previous studies we find low mass halos with high background densities to be more concentrated compared to their low density counterparts of the same mass. Again, this behaviour is reversed for halo masses above $\sim 10^{13} h^{-1}M_{\odot}$ (cf., Wechsler et al. 2006; Gao & White 2007; Jing et al. 2007; Macciò et al. 2007; Wetzell et al. 2007; Angulo et al. 2008; Faltenbacher & White 2009).

The right hand panel of Figure 1 depicts the three dimensional velocity dispersion of the host halos as a function of mass and environment. Low mass halos in high density regions have higher velocity dispersions compared to their counterparts in low density regions. This behaviour is reversed for higher masses which is similar to what is seen for the concentrations. The analog behaviour of concentration and velocity dispersion is in agreement with predictions based on the Jeans equation (e.g., Faltenbacher & Mathews 2007). However, we notice the crossing takes place at some lower masses than seen for the concentrations.

3.2 Accretion history and dynamical structure of satellite systems

The upper left panel of Figure 2 displays the average accretion redshift of satellites within host halos at high (red line) and low (blue line) densities as a function of mass. For hosts below the typical collapse mass, $M_* = 6.15 \times 10^{12} h^{-1}M_{\odot}$, satellites in high density regions are accreted earlier compared to satellites in low density regions. For host masses above M_* the difference becomes marginal or may even reverse. The behaviour of satellite accretion times resembles that of halos themselves (e.g., Gao et al. 2005).

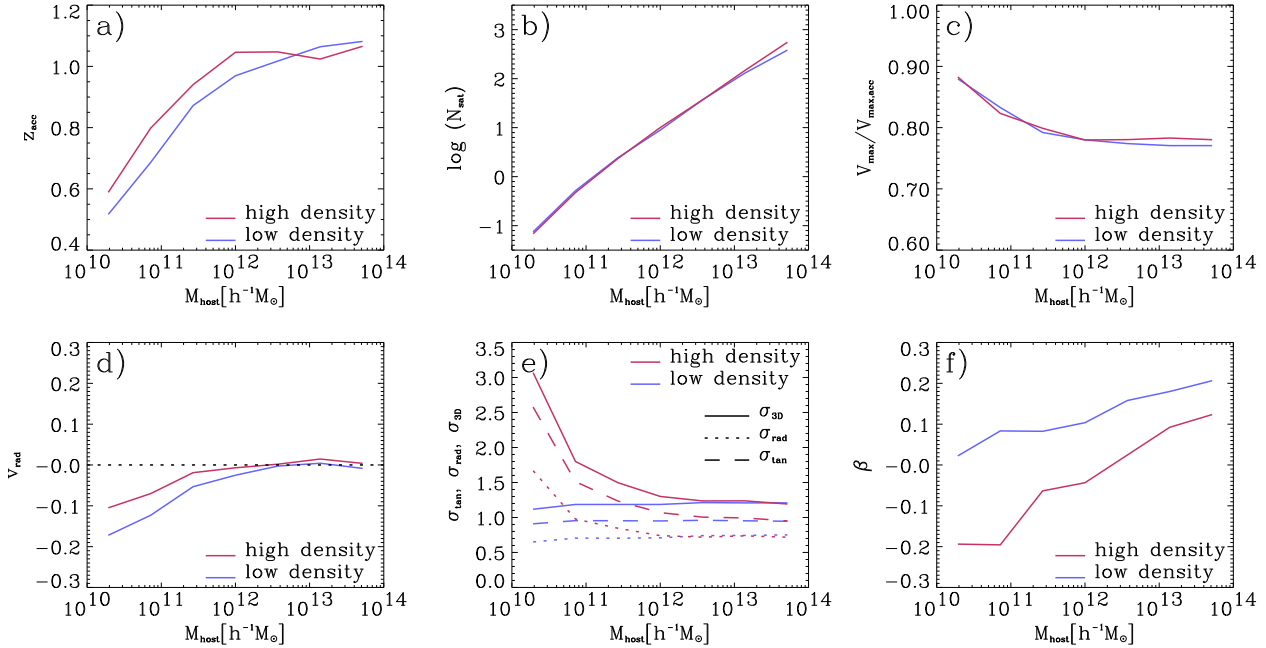


Figure 2. Average sub-halo halo properties, redshift of accretion (z_{acc}), number of sub-halos per host halo (N_{sat}), the ratio of the current maximum circular velocity and its values at the time of accretion ($V_{\text{max}}/V_{\text{max,acc}}$), the radial velocity (v_{rad}), the three dimensional velocity dispersion (σ_{3D}) and the velocity anisotropy β as a function of the host halo mass. Red and blue lines display results based on host halos in the upper and lower 33% tails of their background density distributions. Before averaging the velocity of each individual sub-halo is scaled by the virial velocity of its host halo.

The mean number of satellites for the given host halo masses does not depend on environment as the overlapping graphs in the upper middle panel of Figure 2 indicate. As shown in the upper right panel the average decrease of the maximum circular velocity is about 20% which reduces to 10% for low mass hosts. The central profiles of satellite halos remain fairly intact on their orbits within the potential well of the host. This behaviour is in a agreement with the study by Kazantzidis et al. (2004), see also Boylan-Kolchin et al. (2009).

The lower left panel of Figure 2 depicts the mean radial velocity of satellites as a function of host mass and environment. All velocities are scaled by the corresponding virial velocity. A radial velocity about of zero indicates that on average the satellite distribution is static which is observed for host halos above $\sim 5 \times 10^{11} h^{-1} M_{\odot}$. Negative values correspond to an net infall or some other excess of inward moving satellites.

The lower middle panel in Figure 2 displays the 3D (solid lines) velocity dispersion of satellites and their radial (dotted lines) and the tangential (dashed lines) as a function of host mass and environment. All satellite velocities are scaled by the corresponding virial velocity before averaging. We find a remarkable rise in the dispersions of the satellites in low mass hosts at high densities. These satellites show velocities a few times larger than the virial velocity. This behaviour will be analysed more thoroughly below when we discuss Figure 3.

The lower right panel of Figure 2 presents the anisotropy parameter of satellite galaxies as a function of host mass and environment. We find a profound difference in

the dynamical structure of satellite systems in high density environments as compared to their counterparts at low background densities ($\Delta\beta \geq 0.1$). Independent of host mass, the satellite velocities in low density environments are more radially biased than those in high density regions. Besides the dependence on environment there is also an obvious trend with host mass. Independent of environment, the velocity structure of satellites is more radially biased within more massive hosts.

Host halos in a low density environments dominate the ambient gravitational field more strongly than their equal mass counterparts at high densities. The gravitational field lines point radially towards the host and so does the acceleration exerted on future satellites. The dynamical structure of the satellites within the host halo is a result of the fairly radial inflow. In contrast, the gravitational field in high density regions is more complex. Before satellites are accreted onto a host they also experience non radial accelerations from other massive haloes nearby. As a result the velocities of satellites show a larger non-radial component. The dependence of β on mass may be interpreted in the same way. The more massive the host the more radial the gravitational acceleration of future satellites. Which results in the more radially biased velocity dispersions of the satellites within high mass hosts.

Figure 3 further explores the large velocity dispersion of satellites in low mass hosts at high background densities. Here we display the three-dimensional velocity dispersion of the satellites scaled by the measured three dimensional velocity dispersions of the host halos and not, as in Fig-

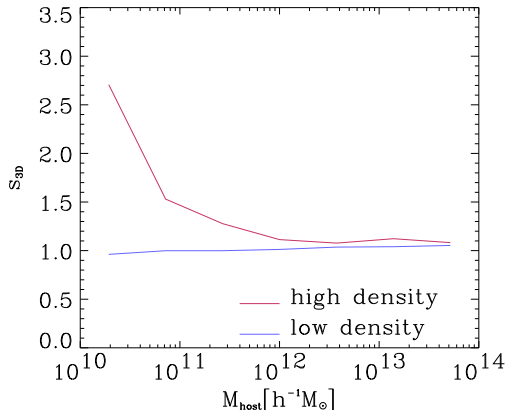


Figure 3. Satellite velocity dispersion scaled by the host halo velocity dispersion, s_{3D} , as a function of host halo mass. Except for the scaling this figure repeats the solid lines in the velocity dispersion panel of Fig. 2.

ure 2, by the virial velocities. Thus, the velocity dispersion of the satellites are directly compared to that of the host. We find that satellites in host halos at low densities and satellites in high mass hosts (independent of environment) don't show velocity bias. This is in agreement with results in Faltenbacher & Diemand (2006) and Lau et al. (2009). The velocity dispersion of satellites in high density environments strongly deviates from this behaviour. For host masses below $\sim 10^{12} h^{-1} M_{\odot}$ the satellites are hotter than the overall dark matter component.

This effect can not be explained by more recent accretion times since, in this case, the low density satellites should show even larger dispersions. Recently, Fakhouri & Ma (2009b) reported on dynamically hotter ambient environments for halos in high density regions. Thus, satellites which merge onto or pass through the host systems are hotter compared to their counterparts at low densities. Low mass hosts in dense environments are located next to more massive halos. These halos expel a substantial fraction of their sub-halos out to large radii (e.g., Gill et al. 2004; Ludlow et al. 2009). It seems plausible that some of these migrant satellites penetrate into low mass hosts and cause their satellites' velocity dispersion to rise. In other words, some fraction of satellites in small mass hosts at high densities do originally not belong to the Lagrangean volume of the host halo instead they got expelled from more massive halos nearby. Those interlopers are dynamically hotter than the host itself.

3.3 Resolution effects

Figure 4 iterates the analysis presented in Figure 2 with the only difference that the restriction on the maximum circular velocity at the time of accretion, $V_{\max, \text{acc}} \geq 30 \text{ km s}^{-1}$, is suspended. Thus, all satellites which can be detected, i.e. all sub-structures which have more than 20 particles, contribute to the results. If a sub-halo falls below the 20 particle limit we consider it as tidally *dissolved*. Tidal dissolution is more prominent in the unrestricted sample. This is the key difference between the satellite sample with and without re-

striction. In the following we discuss the individual panels in Figure 4 and compare them to the corresponding panels in Figure 2:

- a)** The average accretion redshift, z_{acc} , is reduced for the unrestricted sample. This is expected since small mass satellites have shorter survival times. Thus, a large fraction of early accreted low mass systems is missing. However, the dependence on environment persists;
- b)** The average number of satellites increases by a factor of $\lesssim 10$. This is a consequence of the shape of the (sub-)halo mass function (Boylan-Kolchin et al. 2009);
- c)** The average fraction between current maximum circular velocity and that at the time of accretion, $V_{\max}/V_{\max, \text{acc}}$ is increased. This behaviour reflects the low average accretion redshift for the unrestricted satellite sample;
- d)** The average radial velocities, v_{rad} , are negative for all host masses. This is a consequence of the lower mass limit induced by the 20-particle-threshold of the SUBFIND algorithm. As demonstrated in Faltenbacher & Mathews (2007) small mass satellites are most likely to fall below the resolution limit at their peri-centre passage causing an excess of negative radial velocities or inward moving satellites;
- e)** The average velocity dispersions, σ_{3D} , σ_{rad} and σ_{tan} , increase by $\sim 10\%$, independent of mass and environment. In addition there is a substantial rise in the velocity dispersions of satellites in low mass hosts at high densities. The former effect can be explained by the lower average accretion redshifts. More specifically, the increase of velocity dispersion is a result of the tidal dissolution of earlier accreted satellites which have on average lower velocities. After their dissolution the slow moving satellites do not contribute to the overall dispersion anymore which causes a positive bias of the velocity dispersion. This effect is more noticeable for the satellite sample without restriction of $V_{\max, \text{acc}}$ since there tidal dissolution is more prominent. The increase of the velocity dispersion in low mass systems at high density is presumably due to a more intense contamination by interlopers;
- f)** The velocity anisotropy parameter, β , decreases by ~ 0.05 , i.e. the tangential velocity component of the satellites is slightly increased for the sample without restriction on $V_{\max, \text{acc}}$. In addition, one finds a distinct upward turn for low mass hosts in dense environments. The former is due to the fact that satellites on more radial orbits penetrate deeper into the potential well of the host. Consequently, they are more strongly exposed to tidal forces and get dissolved faster. The remaining satellite population is biased towards a more prominent tangential velocity component. The upward trend for low mass hosts at high densities may be explained by interlopers. Dynamically, they are not strongly coupled with the host. Assuming random motions of the interlopers one expects $\beta = 0$ which, in deed, is nearly approached.

The above comparison demonstrates the impact of the finite resolution on the derived dynamical structure of the satellite populations. The 20 particle limit for sub-halos is effectively a mass cut. Satellites which get tidally striped below this limit disappear. This causes a bias towards later accreted satellites and the consecutive effects. In particular the large number of approaching satellites with masses only slightly above the mass cut contributes to the bias. However, if the restriction $V_{\max, \text{acc}} \geq 30 \text{ km s}^{-1}$ is imposed these effects are greatly reduced. In that case the satellites comprise at least ~ 500 particles at the time of accretion. Even sub-

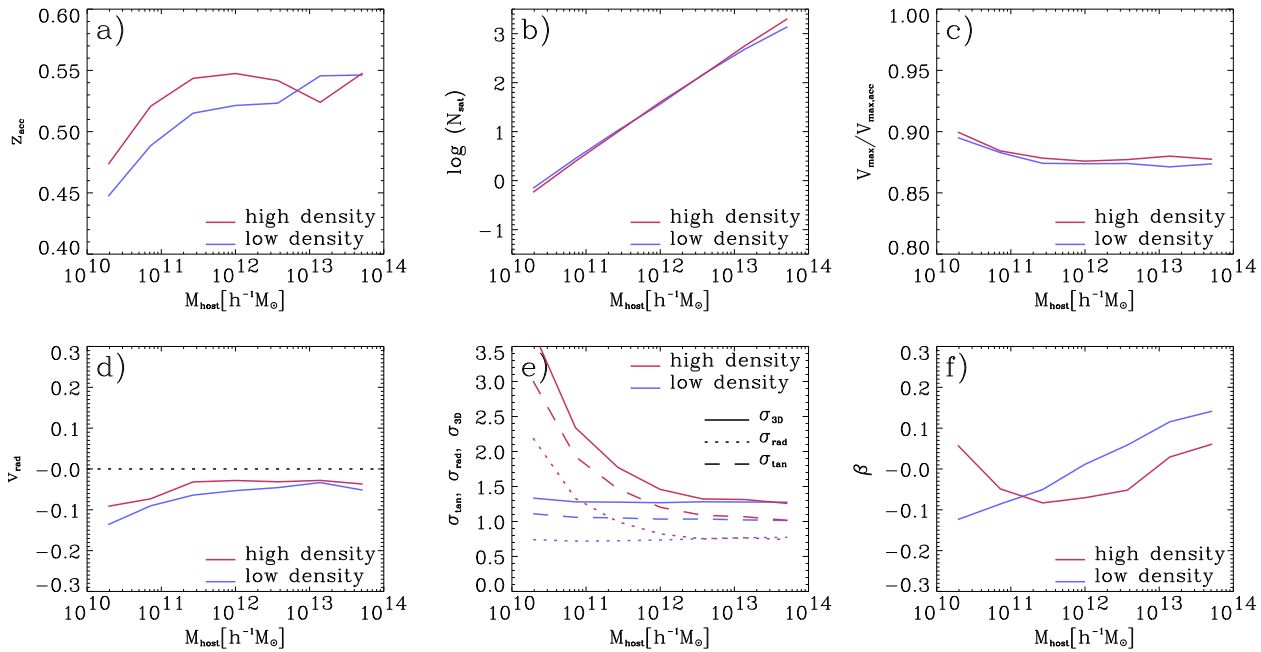


Figure 4. Same quantities as in Figure 2 but based on all satellites, i.e. without any restriction on the maximum circular velocity at the time of accretion.

stantial tidal stripping does not push the satellite below the lower particle limit, i.e. the survival time is only marginally affected by the lower particle limit. Therefore, the results presented in Figure 2 describe physical phenomena and are not caused by the finite resolution of the simulation.

4 CONCLUSION

Taking advantage of the superior resolution of the Millennium-II Simulation we determine the impact of assembly bias on galaxy systems. We conclude with a recapitulation of the main results:

1) The average accretion redshift depends on the host mass and environment. For host masses of $10^{10} h^{-1} M_{\odot}$ we find $z_{\text{acc}} \approx 0.55$ which increases for host halos above $10^{13} h^{-1} M_{\odot}$ to $z_{\text{acc}} \approx 1.05$. The average accretion redshift of satellites halos in high density environments is larger, $\Delta z \approx 0.1$, compared to that of their counterparts in low density regions. The dependence of satellite accretion times on environment reflects what has been known for the overall accretion behaviour of halos in different environments.

2) Host halos above $10^{12} h^{-1} M_{\odot}$ show the same velocity dispersion as their satellite populations. This remains valid for lower mass halos in low density environments. However, the dispersion of satellites within low mass hosts at high densities exceed that of the hosts by a factor of a few. Which may be interpreted as contamination by high velocity interlopers.

3) The velocity anisotropy of satellite halos is correlated with the mass of the host halo. More massive hosts show more radially biased satellite velocities. In addition we find a strong dependence of the velocity anisotropy on environment. Satellite velocities of host halos residing in high density environments tend to be less radially biased

than those in low density environments.

Our findings show that the internal dynamical structure of satellite systems is strongly correlated with environment. We believe that our approach allows to make similar predictions for real satellite galaxy systems. Thus the dynamical structure of satellite galaxy systems should strongly depend on environment. Most notably satellites of host galaxies in less dense environments show a more radially biased velocity structure. This behaviour may have implications for the accretion process of the host galaxies.

ACKNOWLEDGEMENTS

A.F. is grateful to Simon White for helpful comments on the draft of this paper and to Russell Johnston for careful revisions. It is a pleasure to acknowledge South African Astronomical Observatory or kind hospitality. The Millennium-II Simulation databases used in this paper and the web application providing online access to them were constructed as part of the activities of the German Astrophysical Virtual Observatory. Data for halos and galaxies are publicly available at <http://www.mpa-garching.mpg.de/millennium>.

REFERENCES

- Angulo R. E., Baugh C. M., Lacey C. G., 2008, MNRAS, 387, 921
- Bett P., Eke V., Frenk C. S., Jenkins A., Helly J., Navarro J., 2007, MNRAS, 376, 215
- Bond J. R., Cole S., Efstathiou G., Kaiser N., 1991, ApJ, 379, 440

- Boylan-Kolchin M., Springel V., White S. D. M., Jenkins A., 2009, ArXiv e-prints, 0911.4484
- Boylan-Kolchin M., Springel V., White S. D. M., Jenkins A., Lemson G., 2009, MNRAS, 398, 1150
- Cole S., Kaiser N., 1989, MNRAS, 237, 1127
- Dalal N., White M., Bond J. R., Shirokov A., 2008, ApJ, 687, 12
- Fakhouri O., Ma C., 2009a, ArXiv e-prints, 0906.1196
- Fakhouri O., Ma C., 2009b, MNRAS, 394, 1825
- Faltenbacher A., Diemand J., 2006, MNRAS, 369, 1698
- Faltenbacher A., Mathews W. G., 2007, MNRAS, 375, 313
- Faltenbacher A., White S. D. M., 2009, ArXiv e-prints, 0909.4302
- Gao L., Springel V., White S. D. M., 2005, MNRAS, 363, L66
- Gao L., White S. D. M., 2007, MNRAS, 377, L5
- Gill S. P. D., Knebe A., Gibson B. K., Dopita M. A., 2004, MNRAS, 351, 410
- Gottlöber S., Kerscher M., Kravtsov A. V., Faltenbacher A., Klypin A., Müller V., 2002, A&A, 387, 778
- Gottlöber S., Klypin A., Kravtsov A. V., 2001, Progress in Astronomy, 19, 58
- Guo Q., White S., Li C., Boylan-Kolchin M., 2009, ArXiv e-prints, 0909.4305
- Hahn O., Porciani C., Carollo C. M., Dekel A., 2007, MNRAS, 375, 489
- Harker G., Cole S., Helly J., Frenk C., Jenkins A., 2006, MNRAS, 367, 1039
- Jing Y. P., Suto Y., Mo H. J., 2007, ApJ, 657, 664
- Kaiser N., 1984, ApJ, 284, L9
- Kazantzidis S., Mayer L., Mastrogiuseppe C., Diemand J., Stadel J., Moore B., 2004, ApJ, 608, 663
- Kravtsov A. V., Gnedin O. Y., Klypin A. A., 2004, ApJ, 609, 482
- Lacey C., Cole S., 1993, MNRAS, 262, 627
- Lau E. T., Nagai D., Kravtsov A. V., 2009, ArXiv e-prints, 0908.2133
- Ludlow A. D., Navarro J. F., Springel V., Jenkins A., Frenk C. S., Helmi A., 2009, ApJ, 692, 931
- Macciò A. V., Dutton A. A., van den Bosch F. C., Moore B., Potter D., Stadel J., 2007, MNRAS, 378, 55
- Mo H. J., White S. D. M., 1996, MNRAS, 282, 347
- Monaghan J. J., Lattanzio J. C., 1985, A&A, 149, 135
- Navarro J. F., Frenk C. S., White S. D. M., 1997, ApJ, 490, 493
- Press W. H., Schechter P., 1974, ApJ, 187, 425
- Sheth R. K., Tormen G., 2004, MNRAS, 350, 1385
- Springel V., 2005, MNRAS, 364, 1105
- Springel V., White S. D. M., Tormen G., Kauffmann G., 2001, MNRAS, 328, 726
- Springel V., Yoshida N., White S. D. M., 2001, New Astronomy, 6, 79
- Wechsler R. H., Bullock J. S., Primack J. R., Kravtsov A. V., Dekel A., 2002, ApJ, 568, 52
- Wechsler R. H., Zentner A. R., Bullock J. S., Kravtsov A. V., Allgood B., 2006, ApJ, 652, 71
- Wetzel A. R., Cohn J. D., White M., Holz D. E., Warren M. S., 2007, ApJ, 656, 139
- Zentner A. R., 2007, International Journal of Modern Physics D, 16, 763